Received March 11, 2015, accepted May 18, 2015, date of publication July 30, 2015, date of current version August 21, 2015.

Digital Object Identifier 10.1109/ACCESS.2015.2461551

Development of Substrate-Integrated Waveguide Filters for Low-Cost High-Density RF and Microwave Circuit Integration: Direct-Coupled Cavity Bandpass Filters With Chebyshev Response

YU (FREEMAN) TANG[1], KE WU[1], (Fellow, IEEE), AND NAZIH KHADDAJ MALLAT[2], (Senior Member, IEEE)

[1]Poly-Grames Research Center, École Polytechnique de Montréal, Montréal, QC H3T 1J4, Canada
[2]College of Engineering and Information Technology, Al Ain University of Science and Technology (AAU), P.O. Box 64141, Al Ain, United Arab Emirates

Corresponding author: N. Khaddaj Mallat (nazih.mallat@aau.ac.ae)

This work was supported in part by the PolyGrames Research Center, École Polytechnique de Montréal, Montréal, QC, Canada, in part by the Al Ain University of Science and Technology, Al Ain, United Arab Emirates, and in part by the Natural Sciences and Engineering Research Council of Canada.

ABSTRACT Direct-coupled cavity bandpass filters with Chebyshev response are studied and realized, using the technique of planar substrate-integrated waveguide (SIW) for the purpose of high-density integration and cost reduction. Using a general mode-matching technique, the scattering matrix of waveguide bifurcation-type discontinuity and asymmetric iris are established and analyzed. Such discontinuities are used as coupling components and building blocks in the design of filters that are realized on RT/duroid 6002 with the ordinary printed circuit board process in our work. Measurement for one of the three four-pole filters gives 3.4 dB insertion loss and 17 dB return loss over the whole passband at near 24 GHz (*K*-band) with 440-MHz bandwidth (1.8%). The design method can be widely adopted for the development of microwave-integrated circuits, and the mass-fabrication of such SIW filters can be made easy while maintaining a very low cost.

INDEX TERMS Substrate integrated waveguide (SIW), band-pass filter, Chebyshev response function, dielectric loss, and conductor loss.

I. INTRODUCTION

The traditional and most common method used to design planar filter is microstrip line, which supplies lower Q factor and hence higher insertion loss. However, current trends in the development of RF, microwave and millimeter-wave circuits and systems including antennas are being oriented towards the low-cost and high-density integration of front-end circuits and radiating components and elements. This is now mainly driven by the invention and development of the concept of Substrate Integrated Circuits (SICs), in particular, the substrate integrated waveguide (SIW), which allows for the design of usually three-dimensional waveguide circuits and antennas in planar form, thus making possible a complete integration in a single fabrication process of planar and non-planar circuits made of a single substrate.

Power dividers, couplers, filters, antennas, oscillators and other passive and active circuits with this kind of integration platform have been designed and demonstrated. Transitions between the SIW and other planar transmission lines have also been studied and successfully used in practical applications. The performance of the developed components has confirmed the effectiveness and superiority of this new method, which can be used at low cost and for mass production.

In this paper, the design of SIW filter concept is presented for the 24-GHz application with low-cost microwave circuit. The basic structure and design properties of the SIW guides are investigated and discussed with reference to various thicknesses of substrate, loss tangents of material, and relative permittivity of different materials. Three examples of Chebyshev-type band-pass filters of different structures

realized with planar SIW technique are demonstrated and characterized.

II. PROPERTIES OF SUBSTRATE INTEGRATED WAVEGUIDE

Apart from the surface roughness of the SIW guide, which are generally pronounced at up-millimeter-wave and terahertz ranges, the loss usually comes from two mechanisms, namely imperfect conductor wall and dielectric dissipation loss. In these SIW filter designs, periodic circular via holes are not used. Instead, metalized slots are used. Only at cavity corners, the slots cut off the conductive walls, where the vertical currents are actually almost vanished.

The attenuation constants related to imperfect conductors (α_c) and dielectric loss (α_d) in rectangular waveguide, are, respectively [1],

$$\alpha_c = \frac{2R_m}{bZ_0'\left(1-\frac{k_c^2}{k_0'^2}\right)^{1/2}} \times \left[\left(1+\frac{b}{a}\right)\frac{k_c^2}{k_0'^2} + \frac{b}{a}\left(\frac{1}{2}-\frac{k_c^2}{k_0'^2}\right)\left(\frac{ab}{a^2+b^2}\right)\right] \quad (1)$$

and

$$\alpha_d = \frac{k_0'^2 \tan\delta_l}{2\beta_{10}'} \quad (2)$$

where

- R_m is the surface resistance
- $k_0' = k_0\sqrt{\varepsilon_r}$ is the wave number in the dielectric
- $k_c = \frac{\pi}{a}$ is the cut-off wave number
- β_{10}' is the phase constant
- $Z_0' = \sqrt{\frac{\mu_0}{\varepsilon_0}}/\sqrt{\varepsilon_r}$ is the intrinsic wave impedance of the dielectric medium
- ε_r is the relative permittivity of the dielectric material
- $\tan\delta_l$ is the loss tangent of the dielectric material
- a and b are the SIW guide width and thickness (height), respectively.

The units of α_c in (1) and α_d in (2) are Neper/m.

The insertion loss of an SIW waveguide is

$$IL = 10\log_{10}\frac{P}{P_0} = -8.69\alpha_L L \ \ dB \quad (3)$$

where $P = P_0 e^{-2\alpha_L z}$, $\alpha_L = \alpha_c + \alpha_d$ and $P_0 = P|_{z=0}$.

P refers to the power; z is the direction of the wave propagation, and L the length of the SIW guide. Since the loss on the wall of coupling components in the filter is not considered in this analysis, Equations (1), (2) and the resulting IL value (3) give out the minimum loss of the SIW filter of length L, which can be an approximation for our purpose. The unloaded quality factor of a half wavelength cavity is

$$Q_u = \frac{\beta}{2(\alpha_c+\alpha_d)} = \frac{Q_c Q_d}{(Q_c+Q_d)} \quad (4)$$

where $Q_c = \frac{\beta}{2\alpha_c}$ and $Q_d = \frac{\beta}{2\alpha_d}$ are the quality factors in connection with conductive loss and dielectric loss, respectively.

TABLE 1. Attenuations of H_{10} mode in RT/Duroid 6002 SIW structures and Q_u of the half-wavelength cavities.

b (mil)	10	20	30	60
$\alpha_d\ (neper/m)$	0.629	0.629	0.629	0.629
$\alpha_c\ (neper/m)$	0.594	0.309	0.214	0.120
$\alpha_L\ (neper/m)$	1.22	0.938	0.844	0.750
Q_c	595.9	1145	1651	2935
Q_d	563.0	563.0	563.0	563.0
Q_u	289.5	377.5	419.9	472.4

$f_0 = 24GHz, a = 252mil, \varepsilon_r = 2.94$
$\varepsilon_r = \varepsilon_r'(1 - j\tan\delta_l) = 2.94(1 - j0.0012)$

TABLE 2. Attenuations of H_{10} mode in ceramic-filled SIW structures and Q_u of the half-wavelength cavities.

b (mil)	10	20	30	60
$\alpha_d\ (neper/m)$	0.096	0.096	0.096	0.096
$\alpha_c\ (neper/m)$	1.13	0.610	0.437	0.268
$\alpha_L\ (neper/m)$	1.230	0.706	0.533	0.364
Q_c	568.9	1058	1477	2409
Q_d	6699	6699	6699	6699
Q_u	524.5	913.5	1210	1772

$f_0 = 24GHz, a = 137mil, \varepsilon_r = 9.9$
$\varepsilon_r = \varepsilon_r'(1 - j\tan\delta_l) = 9.9(1 - j0.0001)$

Table 1 and Table 2 list the values of those losses with respect to the two kinds of mechanism in a dielectric filled copper waveguide for two different widths, a = 252 mil and a = 137 mil, respectively.

Increasing the thickness of substrate may reduce the conductive loss which results in an increase of the unloaded Q. The design point of the SIW guide in this work is in the first column of Table 1, where the unloaded Q is 289. If 10 mil thick alumina ceramic is used, the unloaded Q may increase to 524. This may be seen in Table 2.

The relationships of the quality factor with reference to the substrate thickness of RT/Duroid 6002 and the loss tangent are plotted in Fig. 1 and Fig. 2, respectively. The relationship of the unloaded quality factor with regards to the substrate

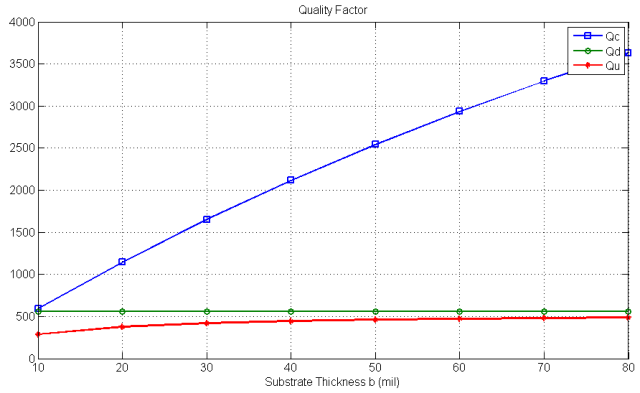

FIGURE 1. Quality factors versus substrate thickness b: a = 252 mil, RT/Duroid 6002.

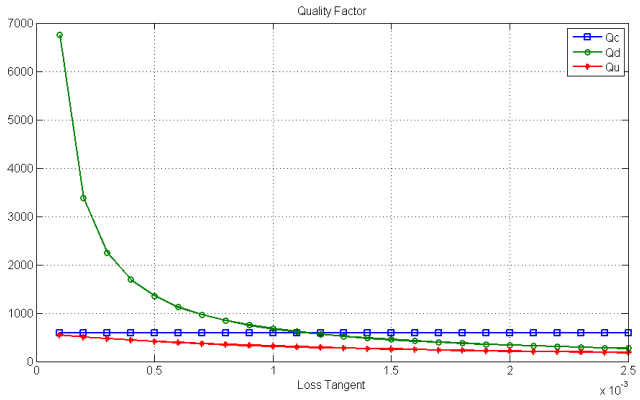

FIGURE 2. Quality factors versustan δ_l: a = 252 mil, b = 10 mil, $\varepsilon_r = 2.94$, $\sigma = 5.8 \times 10^7 S/M$.

thickness in different coating conditions and the relationship of the unloaded quality factor with respect to the tangent loss under different coating conditions are also calculated [7].

III. INDUCTIVE DISCONTINUITIES AND MODE MATCHING MODEL FOR FILTER COUPLING SECTIONS

A. INDUCTIVE DISCONTINUITIES

In the generalized Equation [3] for designing waveguide filters, the impedance (K) or admittance (J) inverter represents the coupling while the half wavelength resonant cavities are in series or cascaded in a line. Shunt inductive discontinuities of waveguide are employed in the configuration as the coupling part. In this paper, the discontinuities of the square shape in the H-plane are handled as shown in Fig. 3.

B. MODE MATCHING TECHNIQUE FOR MODELING SIW DISCONTINUITIES

The solutions of the S parameters to the step-type waveguide discontinuity (junction) and waveguide bifurcation have to be found, which are critical for the modeling and synthesis of SIW filter structures. A single waveguide step discontinuity and an infinitely long waveguide bifurcation are shown in Fig. 4. Let us suppose that an incident H_{10} wave is injected from left into waveguide "a". Forward- and backward-scattering happens at the discontinuity. To meet the boundary condition, higher modes are produced in the vicinity of the discontinuity. In the case of SIW structures where the side walls may be synthesized with two arrays of periodic metallic posts, the guided-waves may be simply formulated by TE modes as TM modes are forbidden to propagation along such structures. This is because the side walls do not allow the flowing of current in the propagation direction, which is different from the conventional rectangular waveguide.

The scattering matrix representation of the waveguide with a single step or bifurcation can be obtained by the technique of mode matching [4]–[6]. When two discontinuities arise, such as the form in Fig. 3, the wave interaction between the two steps (junctions) has to be considered. In the situation of single mode propagation, the incident H_{10} wave from the left is scattered at junction 1. In practice, the wave is often evanescent in the portion between junction 1 and junction 2.

When the waveguide junction and the waveguide portion between junction 1 and junction 2 are represented by the scattering matrix (or ABCD matrix), the overall scattering properties can be represented as the multiplicity of three ABCD matrices [5], [6].

The Wexler model is adopted for calculating the discontinuities in this paper. Instead of calculating the scattering parameters of the discontinuities, the equivalent circuit for the double-plane discontinuities at the band-pass filter

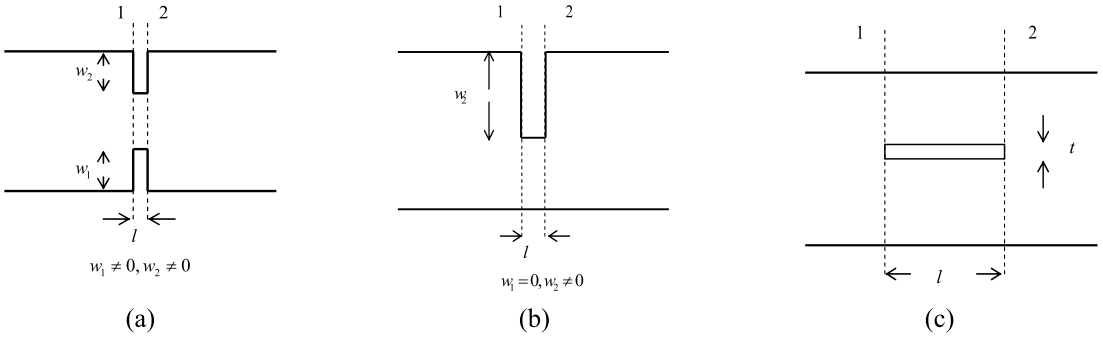

FIGURE 3. Top view: A pair of inductive discontinuities employed as planar filter coupling parts in rectangular waveguide. (a) Symmetric iris. (b) Asymmetric irises. (c) Centrally located bifurcation (axial strip).

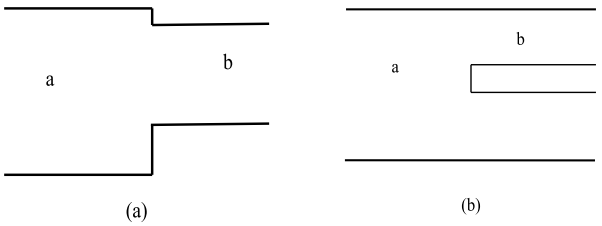

FIGURE 4. (a) Single waveguide step. (b) Infinite waveguide bifurcation.

central frequency is obtained by making use of the symmetry in Fig. 3(a), (b) and (c).

IV. WEXLER MODEL FOR DOUBLE-PLANE STEP-TYPE DISCONTINUITIES

A. WEXLER MODEL

The junction can be described as a function of two transverse coordinates u_1 and u_2. Boundary conditions, the continuity of the transverse fields through all the apertures and a zero tangential electric field at the conducting surface are satisfied by a suitable infinite series of modes appropriate to each side of the junction. A more general situation than those in Fig. 3 is demonstrated in Fig.5. The total transverse electric-field and transverse magnetic field within the aperture at the discontinuity can be expressed in terms of eigenmodes in both guide "a" and guide "b". After manipulating the cross product and applying its orthogonality and normalization properties, the problem becomes one of solvable linear equations [4].

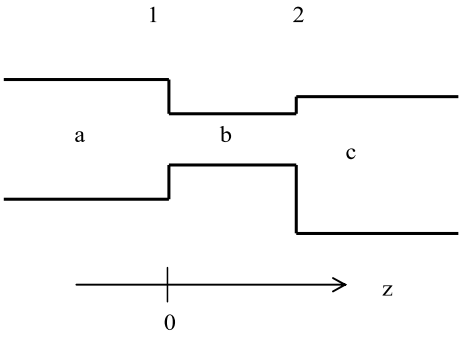

FIGURE 5. Generalized waveguide double-plane steps.

For practical reasons, the infinite series were truncated at M and N, which signify the number of modes in waveguides "*a*" and "*b*", respectively. For complicated problems (e. g. junctions between rectangular and circular guides, etc), the integration in the linear equations should be performed numerically. In this paper, the integrations can be completed in analytical formula. The junction can be represented by T, Π, or transformer networks [2], [8], [9].

B. SYMMETRY CONSIDERATIONS

Symmetries simplify the integrations. For example, the thick irises and finite length bifurcation in Fig. 3 are symmetrical about a transverse plane. If both ports are excited symmetrically, an open circuit appears in the central plane across the coupling part; anti-symmetrical excitation produces a short circuit [2]. In these conditions, pure reflection occurs only in the central plane, and so $s_{jk} = 0$ when $j \neq k$. s_{jj} is given simply by

$$s_{jj} = \frac{1 - y'_{bj}}{1 + y'_{bj}} \tag{5}$$

where y'_{bj} is the normalized input admittance of the j^{th} mode in b at the point of discontinuity, distance $l/2$ from the equivalent plane. Therefore, two parameters are sufficient to specify the equivalent network of such discontinuities, as shown in Fig. 6. The computed input impedance with symmetric excitation, yields $Z_{11} + Z_{12}$, and that with anti-symmetric excitation gives $Z_{11} - Z_{12}$.

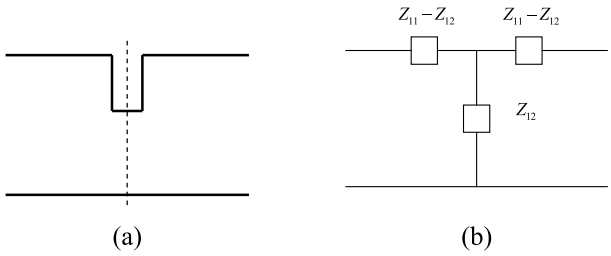

FIGURE 6. (a) Symmetry of the iris. (b) The equivalent circuit of the discontinuities.

C. SIMPLIFIED FORMULA FOR THE INTEGRATIONS

1) CASE 1 (H-PLANE BIFURCATION)

Fig. 7 shows a rectangular waveguide loaded with a thick conducting vane. The Y-coordinate dimensions are normalized with respect to the broad dimension a ($= w$). Assuming excitation by an H_{10} mode, only symmetrical modes are generated at the discontinuity in guide "a".

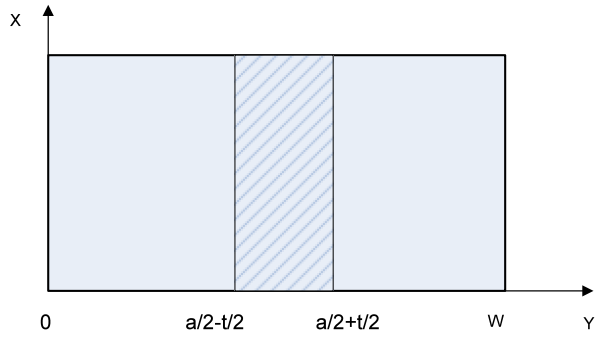

FIGURE 7. Centrally located bifurcation of thickness of t in a rectangular waveguide (guide width $a = w$).

The expressions for the transverse field and the wave admittance of the modes in guides "a" and "b" can easily be obtained [4].

For the structure in Fig. 4(b), the s_{jk} terms are vanishing due to the infinite length of the bifurcated guide. The linear equations were solved in a Matlab environment.

Forward- and back-scattered mode coefficients were computed and, from the reflection coefficient ρ, the normalized

input admittance seen from guide "a" at the junction was computed by

$$y' = \frac{1-\rho}{1+\rho} \tag{6}$$

After obtaining the forward-scattered mode coefficients b_j/a_1 and the backward-scattered mode coefficients a_i/a_1, the apportionment of power between the scattered modes can be calculated.

The normalized input admittance of the j^{th} mode, distance $l/2$ from an open circuit at the central plane, is

$$y'_{bj} = \tanh(\gamma_j l/2) \tag{7}$$

and with a short circuit at the central plane

$$y'_{bj} = \coth(\gamma_j l/2).s_{jj} \tag{8}$$

is then computed.

2) CASE 2 (THICK ASYMMETRIC IRIS)

Fig. 8 shows a general situation of the iris structure in the waveguide.

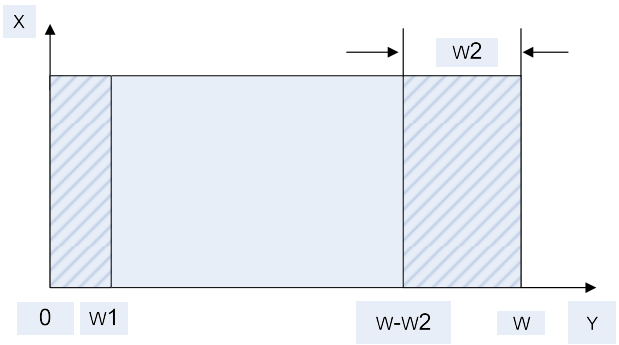

FIGURE 8. Cross-section view: Asymmetric iris.

The transverse field in guide "b" is expressed as,

$$\vec{e}_{bj} = \vec{u}_x \sin(\frac{q\pi y}{w - w_1 - w_2}) \tag{9}$$

$$\vec{h}_{bj} = \vec{u}_y y_{bj} \sin(\frac{q\pi y}{w - w_1 - w_2}) \tag{10}$$

where q is the mode number.

The admittance is,

$$y_{bj} = \sqrt{\frac{\varepsilon_0\varepsilon_r}{\mu_0}}\sqrt{1 - (\frac{q\lambda_0/2}{w - w_1 - w_2})^2} \tag{11}$$

The propagation constant of the j^{th} mode in guide "b" is given by

$$\gamma_j = \frac{\pi}{w}\sqrt{(\frac{q}{1 - \frac{w_1+w_2}{w}})^2 - (2\frac{w}{\lambda_0})^2} \tag{12}$$

Referring to the linear equations in [4], the integrations are given below.

$$\int_a \vec{e}_{ai} \times \vec{h}_{ai} \cdot \vec{u}_z ds = \frac{1}{2} w y_{ai} \tag{13}$$

$$\int_b \vec{e}_{bj} \times h_{bj} \cdot \vec{u}_z ds = \frac{1}{2} y_{bj}[w_1 \frac{\sin(f)}{f} - (w - w_2)\frac{\sin(g)}{g} + w - w_1 - w_2] \tag{14}$$

$$\int_b \vec{e}_{bj} \times \vec{h}_{ai} \cdot \vec{u}_z ds = -\frac{1}{2} y_{ai}\{(w - w_2)[\frac{\sin(f_1)}{f_1} - \frac{\sin(g_1)}{g_1}] - w_1[\frac{\sin(f_2)}{f_2} - \frac{\sin(g_2)}{g_2}]\} \tag{15}$$

where f, g, f_1, f_2, g_1, g_2 have the simple expressions given in [7].

3) CASE 3 (THICK SYMMETRIC IRIS)

Let us set $w_1 = w_2$ in Case 2. The electric field, magnetic field, admittance and propagation constant of j-$^{\text{th}}$ mode in guide "b" were obtained by setting $w_2 = w_1$ in (9), (10), (11) and (12). The integral terms in the linear equations were further simplified. In both guides "a" and "b", only symmetric modes exist. j and k in the linear equations are odd numbers.

D. THE CONVERGENCE OF THE PROBLEM

The boundary value problem involves the calculation of these amplitude coefficients from an appropriate truncation of the expanding terms. Some authors have studied the convergence of the problem. To make the numerical solution very accurate, the number of modes in each waveguide should be enough to reach the true value accurately. For our boundary value problem, there exists the hazard of converging to a relative convergence result [10], [11]. The authors found that, when the ratio of the number of the mode in waveguide "a" to that in waveguide "b" is close to a/b, the numerical solution may avoid the relative convergence problem [5], [9]–[11].

V. DIRECT-COUPLED CAVITY SIW FILTERS

A. FILTER DESIGN

The design method is based on the general synthesis theory for the distributed stepped impedance low-pass prototype [12]–[16]. Wave reflections are produced by inserting discontinuities between the cavities. These discontinuities behave like impedance inverters, i.e. K inverters. The values of the K inverter are given by the explicit formula of Rhode [16]. The design procedure employs Levy's modified formula [5], [17], which can be applied to filters with moderate bandwidth ($\geq 20\%$).

For a lossless junction, the S matrix is unitary and reciprocal. Therefore, the S matrix is uniquely determined by knowing the magnitude and phase of one of its elements, e.g. the reflection coefficient S_{11}. The dimensions of a bifurcation and an iris for a given reflection coefficient can be determined inversely.

B. NUMERICAL RESULTS

1) NUMERICAL RESULTS FROM THE WEXLER MODEL

The vector function superposition of solved transverse electric field amplitude coefficients is shown in Figs. 9 and 10.

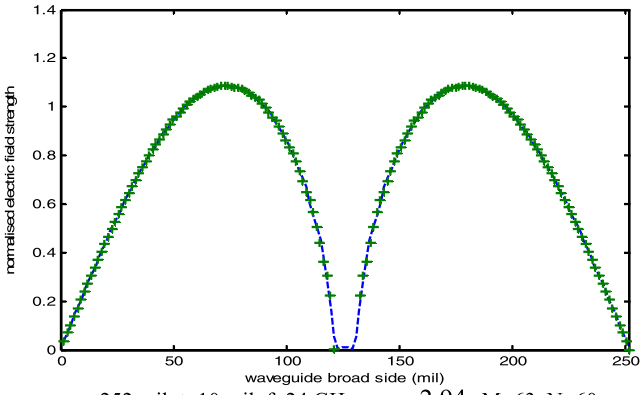

w=252 mil, t=10 mil, f=24 GHz, $\varepsilon_r = 2.94$, M=63, N=60.
Blue: in guide a; green: in guide b

FIGURE 9. Electric field distributions at junction of infinitely long bifurcation.

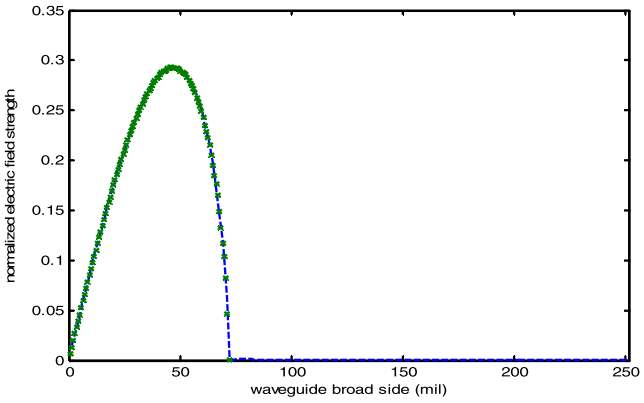

asymmetric iris: w=252 mil, w_1 =0 mil (aperture at left),
w_2 =180 mil; f=24 GHz, $\varepsilon_r = 2.94$, M=141, N=40.

FIGURE 10. Electric field distributions at junction of waveguide step.

The magnetic field amplitude coefficients are also matched perfectly.

2) NUMERICAL RESULTS FOR STRUCTURAL PARAMETERS FROM THE FILTER SYNTHESIS PROCEDURE

Case 1: Metal Insert Configuration ($l > t$)

Specifications are listed in Table 3.

According to the above, the value of n is determined as 4. The rejections at the stop-bands are: $IL|_{f_a} \leq -65dB$ and $IL|_{f_b} \leq -60dB$. The impedance inverters are as follows: $K_{0,1} = 0.1734$, $K_{1,2} = 0.0277$, $K_{2,3} = 0.0219$, $K_{3,4} = K_{1,2}$, $K_{4,5} = K_{0,1}$. The corresponding reflections are: $s_{0,1} = -0.9416$, $s_{1,2} = -0.9985$, $s_{2,3} = -0.9990$, $s_{3,4} = s_{1,2}$, $s_{4,5} = s_{0,1}$; the dimensions of the longitudinal slots are:

$$\begin{cases} t = 10mil \\ l_1 = 70mil \end{cases} \quad \begin{cases} t = 10mil \\ l_2 = 198mil \end{cases} \quad \begin{cases} t = 10mil \\ l_3 = 220mil \end{cases}$$
$$\begin{cases} t = 10mil \\ l_4 = l_2 \end{cases} \quad \begin{cases} t = 10mil \\ l_5 = l_1 \end{cases} \tag{16}$$

The corresponding phase angles due to the coupling components are:

$$\varphi_{0,1} = -1.0203, \quad \varphi_{1,2} = -1.0343, \quad \varphi_{2,3} = -1.0344,$$
$$\varphi_{3,4} = \varphi_{1,2}, \quad \varphi_{4,5} = \varphi_{0,1}$$

Cavity lengths are:

$$cl_1 = 117.45mil, \quad cl_2 = 117.10mil, \quad cl_3 = cl_2,$$
$$cl_4 = cl_1 \tag{17}$$

Case 2: Symmetric bifurcation Configuration ($l < t$)

Specifications: The same as in Case 1.

Calculating with the same procedure, the dimensions of the copper coated transverse slots are:

$$\begin{cases} t_1 = 54mil \\ l = 10mil \end{cases} \quad \begin{cases} t_2 = 116mil \\ l = 10mil \end{cases} \quad \begin{cases} t_3 = 124mil \\ l = 10mil \end{cases}$$
$$\begin{cases} t_4 = t_2 \\ l = 10mil \end{cases} \quad \begin{cases} t_5 = t_1 \\ l = 10mil \end{cases} \tag{18}$$

Cavity lengths are given by:

$$l_1 = 160.13mil, \quad l_2 = 170.20mil, \quad l_3 = l_2, \quad l_4 = l_1 \tag{19}$$

Case 3: Asymmetric Iris Configuration ($w_1 = 0, w_2 \neq 0$)

Specifications are listed in Table 4.

The dimensions of the irises are:

$$\begin{cases} l = 10mil \\ w_1 = 0mil \\ w_{2,1} = 137mil \end{cases} \quad \begin{cases} l = 10mil \\ w_1 = 0mil \\ w_{2,2} = 170mil \end{cases} \quad \begin{cases} l = 10mil \\ w_1 = 0mil \\ w_{2,3} = 175mil \end{cases}$$
$$\begin{cases} l = 10mil \\ w_1 = 0mil \\ w_{2,4} = w_{2,2} \end{cases} \quad \begin{cases} l = 10mil \\ w_1 = 0mil \\ w_{2,5} = w_{2,1} \end{cases} \tag{20}$$

Cavity lengths are given by:

$$cl_1 = 159.66mil, \quad cl_2 = 169.71mil, \quad cl_3 = cl_2,$$
$$cl_4 = cl_1 \tag{21}$$

TABLE 3. Filter specifications - Case 1.

f_0 (GHz)	24	BW(MHz)	340	IL	0.1 dB
f_1 (GHz)	23.83	f_a (GHz)	23	$IL\|_{f_a}$	$\leq -60dB$
f_2 (GHz)	24.17	f_b (GHz)	25	$IL\|_{f_b}$	$\leq -60dB$

TABLE 4. Filter specifications - Case 3.

f_0 (GHz)	24	BW(MHz)	440	IL	0.1 dB
f_1 (GHz)	23.78	f_a (GHz)	23	$IL\|_{f_a}$	$\leq -55dB$
f_2 (GHz)	24.22	f_b (GHz)	25	$IL\|_{f_b}$	$\leq -55dB$

TABLE 5. Optimization results for Case 1.

l_1	cl_1	l_2	cl_2	l_3
25.49	128.15	126.85	127.98	149.83
cl_3	l_4	cl_4	l_5	---
127.98	126.85	128.15	25.49	---

Note: $t = 10mil$, unit in mil

TABLE 6. Optimization results for Case 2.

t_1	cl_1	t_2	cl_2	t_3
26.81	149.21	90.84	166.15	102.69
cl_3	t_4	cl_4	t_5	---
166.15	90.84	149.21	26.81	---

Note: $l = 10mil$, unit in milne

TABLE 7. Optimization results for Case 3.

$w_{2,1}$	cl_1	$w_{2,2}$	cl_2	$w_{2,3}$
125.01	151.61	164.31	176.97	170.84
cl_3	$w_{2,4}$	cl_4	$w_{2,5}$	---
167.97	164.31	151.61	125.01	---

Note: $l = 10mil$, $w_1 = 0$

3) OPTIMIZATION OF THE STRUCTURAL PARAMETERS

The structural parameters were optimized in a software environment, *u-wave wizard*.

The structural parameters in (16) and (17) were optimized and the final values are shown in Table 5.

After optimizing, the parameters in (18) and (19) were as given in Table 6.

And those in (20) and (21) are updated, as in Table 7.

VI. SIMULATION, FABRICATION AND MEASUREMENT

A. SIMULATION WITH FULL-WAVE ANALYSIS

The optimized filters were simulated in an HFSS environment. The loss tangent and metal conductivity in RT/Duroid 6002 were used in the simulation.

Case 1: The simulation results of the metal insert filter are shown in Fig. 11.

Case 2: The simulation results of the wide bifurcation filter are shown in Fig. 12.

Case 3: The simulation results of the asymmetric iris filter are shown in Fig. 13.

In Fig. 13, the transitions are included in the filter simulation while the results in Fig. 11 and Fig. 12 are for the filtering portion only.

The dimensions of the transition with a quarter-wave transformer were obtained through the following procedure [7]. The width $w_1 = 143.6mil$ was determined by the equivalent impedance value defined by the power-current relationship of the SIW guide in an HFSS environment. $w_3 = 25.7mil$ was obtained for the requirement of a 50 Ohm microstrip line on the chosen substrate thickness and with dielectric permittivity. $w_2 = 64.6mil$ was obtained by the requirement of a quarter-wave transformer between the 50 Ohm microstrip line and the wider lower impedance line. The insertion loss of a single transition is about 0.16 dB at the central frequency 24 GHz, and keeps almost the same value at the narrow pass-band edge ($f_1 = 23.8GHz$, $f_2 = 24.2GHz$). The transition with taper is with wider frequency response and much better reflection performance than that of a quarter-wave transformer [7].

In HFSS simulation, the group delays at the filter center frequencies are 1.76 ns, 1.67 ns and 1.4 ns respectively while the minimum insertion losses in the pass band are 3.62 dB, 3.76 dB and 3.4 dB respectively.

B. FABRICATION

The main limitation of SIW used for filter design is the dielectric loss which is relatively high [18], [20]. The PCB process in the Poly-Grames Research Center is implemented

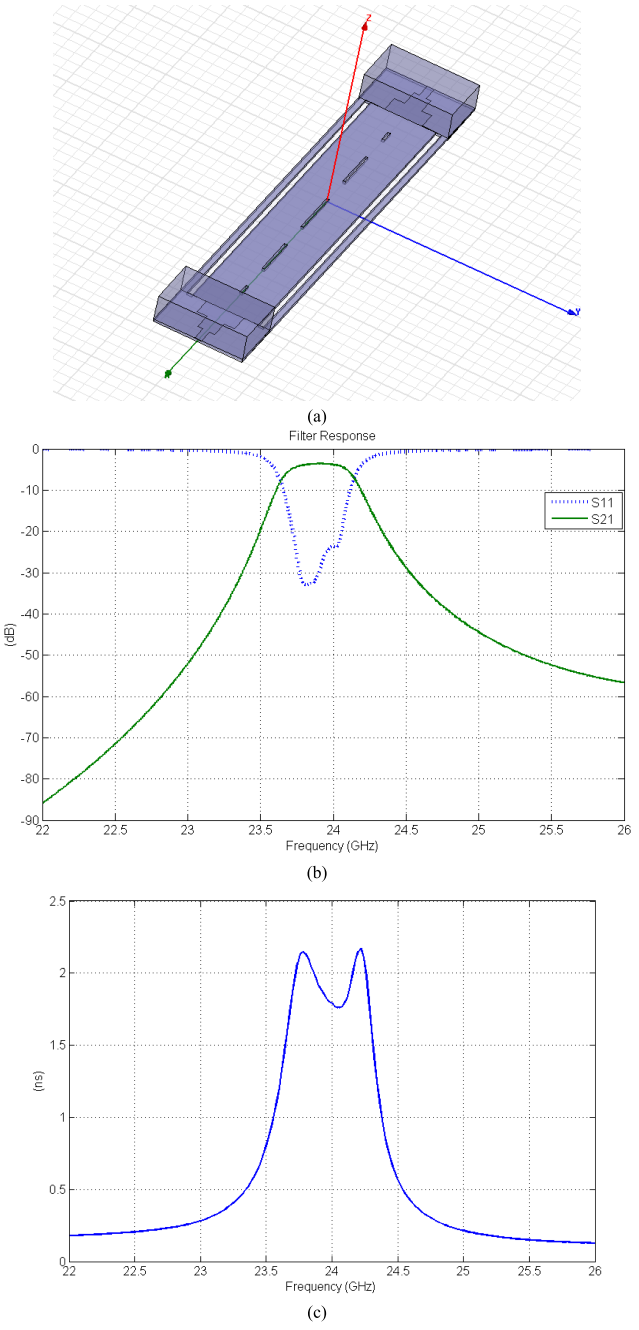

FIGURE 11. Case 1: metal insert filter. (a) HFSS model. (b) Filter response in HFSS. (c) Time delay.

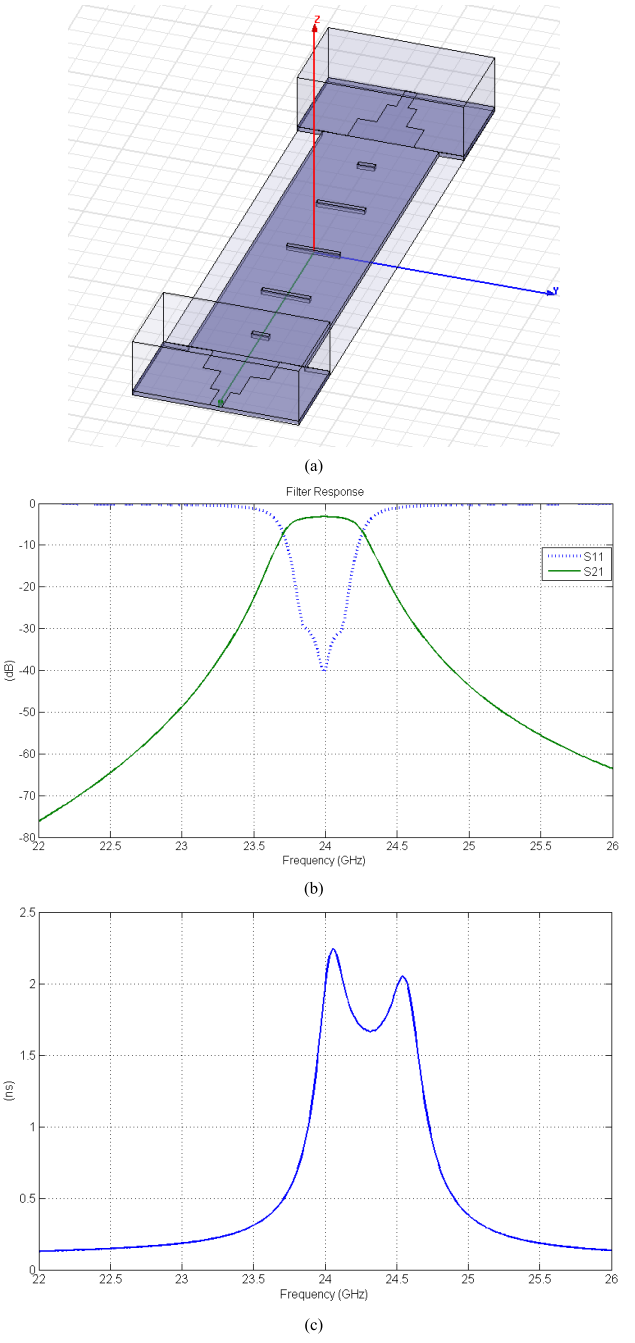

FIGURE 12. Case 2: wide bifurcation filter. (a) HFSS model. (b) Filter response in HFSS. (c) Time delay.

by either laser cutting or drilling. The minimum slot or groove width by laser cutting is about 10 mil. Moreover, this value is confined by the substrate thickness, i.e., the minimum slot width cannot be smaller than the substrate thickness.

A high Q cavity is confidently expected, in order to reduce loss. From Table 2, we may see that conductive loss on the conductor walls predominates over dielectric loss if the tangent loss of the dielectric is very small. For the RT/Duroid 6002, the attenuation constants for both conductor and dielectric loss are shown in Table 1. They are in the same dissipation level in 10 mil thick SIW. Increasing the thickness of the substrate increases Q and reduces the conductor loss of the filter. So a via hole should be used to replace the slot and groove if a thicker substrate (>20 mil) is used [21].

The filters are realized in 10 mil RT/Duroid 6002 substrate. Radiation from the transition design is another factor to confine the integration being realized in 10 and 20 mil substrates. Since the optimization software u-wave had been used for a period of forty days, only filters with coupling parts of 10 mil width were optimized.

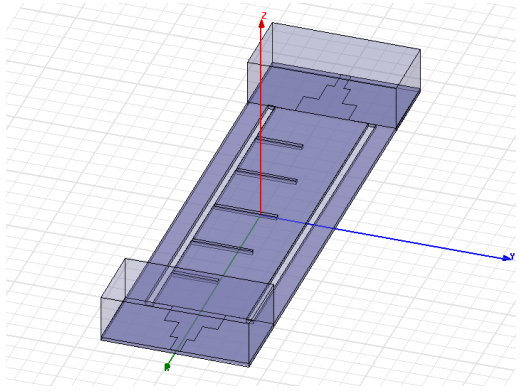

(a)

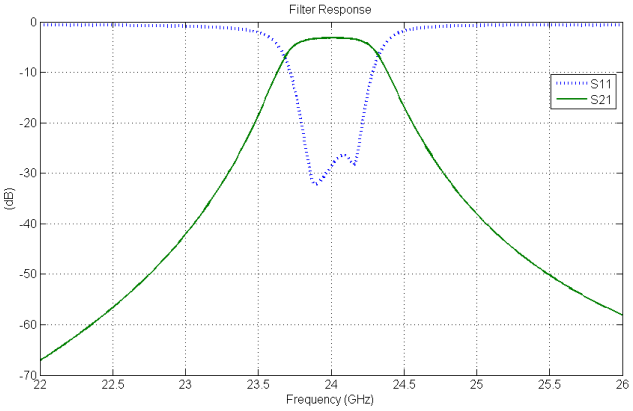

(b)

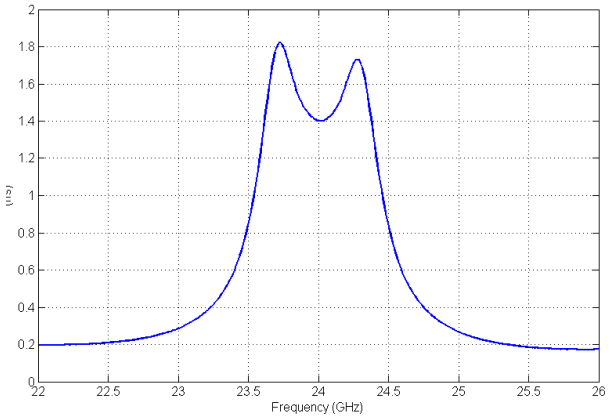

(c)

FIGURE 13. Case 3: asymmetrical iris filter. (a) HFSS model. (b) Filter response in HFSS. (c) Time delay $t_d = \frac{d\varphi}{d\omega} = \frac{1}{2\pi}\frac{d\varphi}{df}$ (22).

C. MEASUREMENTS

The filters in Fig. 11, 12 and 13 were measured after calibrating the HP 8510 Vector Network Analyzer with Open-Short-Load calibration standards. The measurements results of filters with the quarter-wave transformer transitions are shown in Fig. 14, Fig. 15 and Fig. 16, which correspond to Case 1, Case 2 and Case 3 respectively, as described in Section VI.

D. ANALYSIS OF THE FILTERS

The central frequency shifting to 24.36 GHz, 24.32 GHz and 24.38 GHz respectively occurs because of the relative permittivity tolerance or error. The virtual relative permittivity of a Rogers RT/Duroid 6002 laminated substrate is about 2.86. The comparisons between the results of simulation using such values, and the test results of the filters of Cases 2 and 3 are also shown in Figs. 15 and 16, respectively.

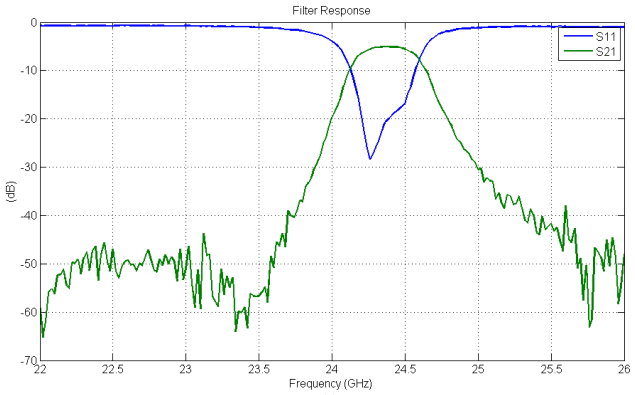

(a)

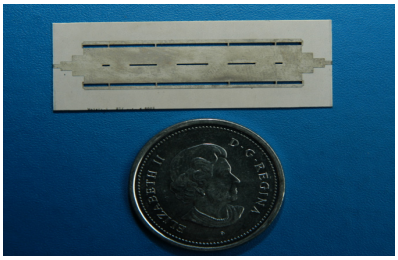

(b)

FIGURE 14. 14 Filter response of "Case 1". (a) Filter response of the metal insert filter. (b) The metal insert filter in SIW realization.

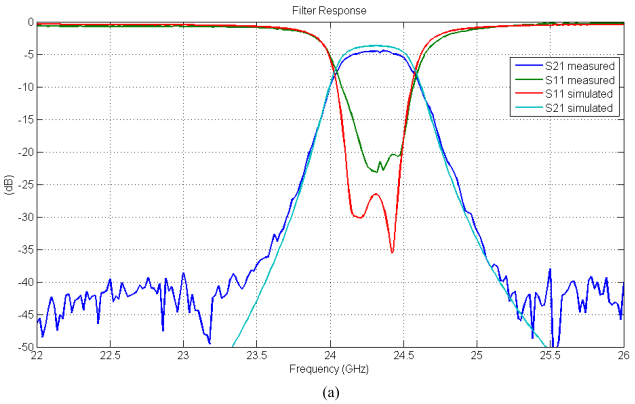

(a)

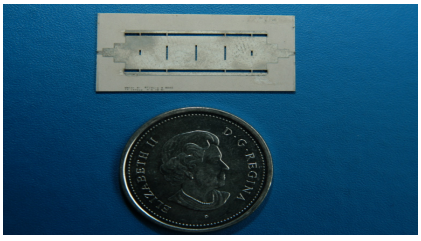

(b)

FIGURE 15. Filter response of "Case 2". (a) Filter response of the wide bifurcation filter. (b) The wide bifurcation filter in SIW realization.

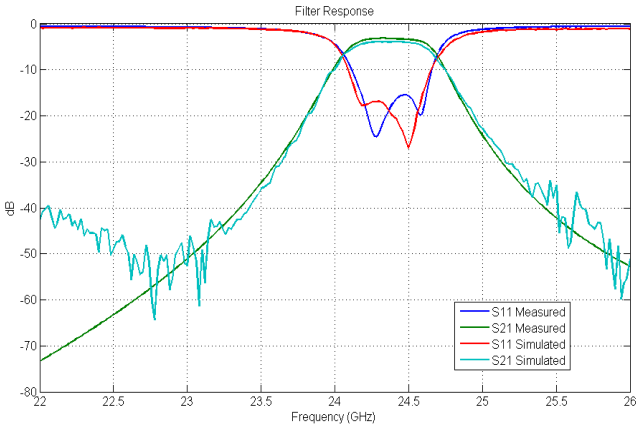

(a)

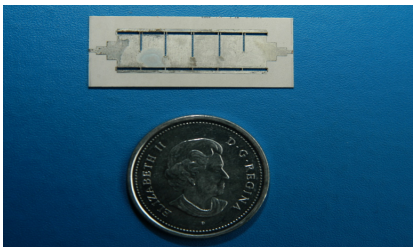

(b)

FIGURE 16. Filter response of "Case 3". (a) Filter response of the asymmetric iris filter. (b) The asymmetric iris filter.

In the pass-band and on the rejection skirts, the test results for the simulated results agree. In the stop-band, the tested transmission rejections are smaller than the simulated ones.

Since Open-Short-Load calibration standards were used to define the reference planes of the tests, the results shown in Figs. 14, 15 and 16 include the additional insertion loss from the test fixture. According to our previous measurements results, the estimated insertion loss of the test fixture is about 0.5 ± 0.1dB at 24 GHz. Therefore, at the central frequencies, the insertion losses are 4.9 ± 0.1 dB, 4.0 ± 0.1 dB and 3.4 ± 0.1 dB respectively.

Case 1 uses long metal insert as coupling structures which gives longer dimension in wave propagating direction. Hence, the filter has longer group delay compared with Case 2 and Case 3. Among the three cases, Case 3 has the best effective cavity geometry and more reasonable coupling parts which supply much better insertion loss.

1) TOLERANCE ANALYSIS

Tolerance analysis was implemented for the asymmetric iris filter and the simulation results are shown in Fig. 17. The broad wall width of the SIW guide, the thickness of the inductive iris in the longitudinal direction and the width of the iris in the transverse direction deviated with an error of $\pm\Delta$. The resonant cavity lengths were deviated as the consequence of the changing thicknesses of the iris. Uniformly distributed random numbers were produced for 20 sets of filter dimensions.

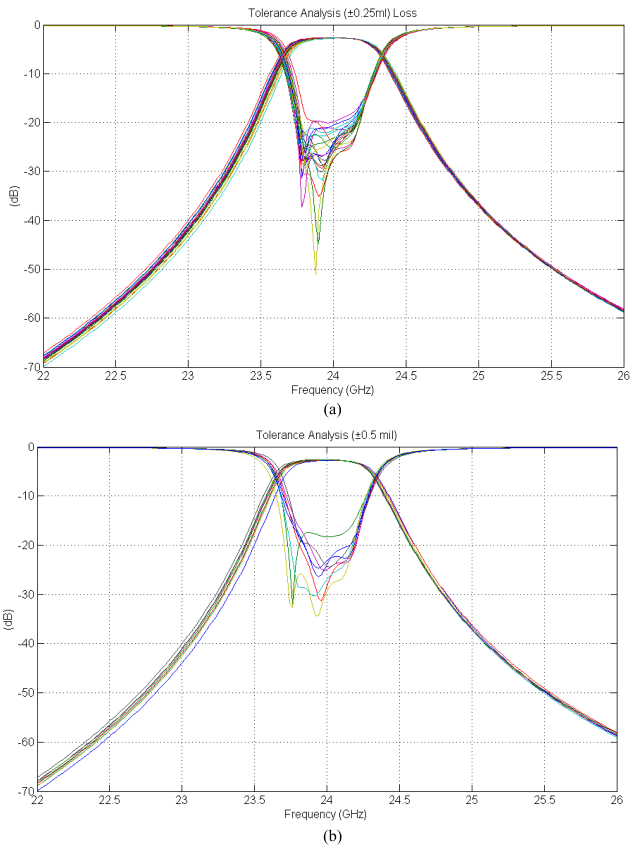

(a)

(b)

FIGURE 17. Tolerance analysis of the asymmetrical iris filter. (a) When $\Delta = 0.25$ mil. (b) When $\Delta = 0.5$ mil.

In order to ensure the minimum filtering characteristics of the structures, a maximum -15 dB of return loss was set between 23.78 GHz and 24.22 GHz. Insertion losses corresponding to this return loss specification keeps strictly confined to the design requirement. When $\Delta = 0.25, 0.5$ mil, the simulated filter responses are shown in Fig. 17 (a) and (b). Throughout these few iterated calculations, the tolerance to ensure the performance of the filter is about 0.4 mil.

2) PULSE POWER CAPABILITY

Operating at potentially high power, filters need to prevent electric field strengths from approaching the breakdown point. With Cohn's method [22], the maximum cavity electric field strengths at the center of the pass-band are given in terms of the electric strength of the matched output waveguide.

The pulse-power capability of the direct-coupled-resonator filter, at the center frequency, is given by [3],

$$(P_{qk})_0 = \frac{P'_{qk}\pi w}{2g_k\omega'_1}\left(\frac{\lambda_{g0}}{\lambda_0}\right)^2 \tag{23}$$

where P'_{qk} is the pulse-power capacity of a matched waveguide having the same cross section as the cavity; g_k and ω'_1 are the element value and equal-ripple band edge for the low-pass prototype of Cohn.

Taking the $g_k = 1, \omega'_1 = 1, w = 1.2\%, \lambda_{g0} = 8.87$ mm and $\lambda_0 = 7.29$ mm into (23), the relative pulse-power capability

TABLE 8. Power flow of SIW guides of 10 mil thick & filter pulse power-capability.

Material	Duroid 6002	Duroid 6006	AlN	Alumina ceramic	Sapphire
ε_r	2.94	6.15	8.9	9.9	11.5
$a \times b(mil)$	252x10	174x10	145x10	137x10	127x10
DBV (KV/cm)	30	62	100	150	180
Power flow (KW)	13.68	58.30	152.21	340.70	489.96
Pulse power capacity (KW)	0.382	1.628	4.242	9.526	13.71

Note: band-width $w = 1.2\%$

$(P_{qk})_0/P'_{qk} = 2.8\%$. The power flow of H_{10} mode in SIW guide is given by [1],

$$P'_{qk} = P_{10} = \frac{|A_{10}|^2\, ab}{4}\left(\frac{\beta'_{10}}{k_{c,10}}\right)^2 Z'_{h,10} \tag{24}$$

Setting the amplitude of E_y as the breakdown voltage of the dielectric (RT/Duroid 6002), the maximum amplitude $A_{10}|_{\max}$ of the longitudinal magnetic vector H_z can be obtained. Taking the value of $A_{10}|_{\max}$ into (24), the maximum power flow of the SIW waveguide is obtained. In this paper, the dielectric breakdown voltage (DBV) of the RT/Duroid 6002 was estimated as $30KV/cm$.

The power capacity of the SIW guide is $P'_{qk} = 13.68KW$ for the waveguide cross-section of $a = 252mil$, $b = 10mil$. Suppose that each cavity has the same power capacity. Simply setting $g_k = 1$ and $\omega'_1 = 1$, since the bandwidth of the narrow-band SIW filter is $w = 1.2\%$, the pulse-power capacity at center frequency $f_0 = 24GHz$ is $(P_{qk})_0 = 382W$. In a safety state, the practical power capacity of a waveguide is usually estimated as one third of the ultimate value. The safety maxim operating power of the SIW filter is 127 W.

The power flow in SIW guides using different substrate material is an interesting perspective on SIW guides. Table 8 lists the values of power flows in various SIW guides.

At the frequencies going away from the center frequency in the pass-band, the power capability decreases. The details of these physical properties are not gone into here. Obviously, the pulse-power capability is proportional to the substrate thickness for the SIW filters.

Keeping the same design specifications of the filter but using different substrate material, the power-capabilities of the direct-coupled cavity filter integrated on 10 mil substrate are listed in Table 8, where all the data were from a bandwidth of $w = 1.2\%$ and by setting $g_k = 1$, $\omega'_1 = 1$ for the low-pass prototype.

The above brief analysis on pulse power capability was done in the past when this project was implemented. It is of even more practical meaning to analyze and calculate the average power handling capability of a SIW filter since the peak power may not reach that high in many applications but the heat effect due to self-heating may greatly deteriorate the average power handling capability. A SIW filter working in its ambient circumstance, with its own heat deposition due to power dissipation, strong E-field component around the slot edge, and heat sink convention condition, its average power handling capability is significantly limited by the temperature rise and hot spots due to self heating. This leads to physical and geometrical dimension changes of SIW filter and hence a filter frequency drift and/or a detuning will occur. An analysis procedure with full-wave simulation is recently implemented on a Ka band SIW filter by X-P Chen [23] and the results on this heat isolated Ka band SIW filter (without heat sink) is demonstrated, considering the main factors including voltage of each cavity across the pass band and stop band, melting of glass in the laminate material and permittivity change due to temperature rise etc. It is also pointed out whether in the stop band or the pass band, microwave breakdown will take place first around the slot edge of the input conductor backed CPW in the case. A work focusing on analyzing the average power handling capability of SIW interconnects using model considering heat sink is also done by Cheng *et al.* [24].

VII. CONCLUSION

Three direct-coupled cavity filters of four cavities are realized with SIW technique on a Rogers RT/Duroid. Measurements have demonstrated that the results agree well with the design theories. The insertion loss of the asymmetrical iris filter reached 3.4 dB. The insertion loss of the other filters was 4.0 and 4.9 dB, respectively. The insertion loss of the filters is relatively high because relatively high tangent loss material was used. This is expected to improve by using high purity

ceramic material whose tangent loss is one tenth of that of RT/Duroid 6002. The reason is the radiation of the relatively wide microstrip structure of the 50 Ohm transmission line. A new design for the transition might solve the problem of integration on a thicker substrate. Increasing the thickness of the substrate may reduce the loss. However, the performance of the transition may be deteriorated with more than 20 mil of thickness. Since the optimization software u-wave wizard had been used for forty days in the present study, a design where the slot width of the coupling parts had to be increased to 20 mil in the process, was not made in our lab. The curves and tables in Section II give guidance for choosing the dielectric parameters.

ACKNOWLEDGEMENTS

The authors thank Roch Brassard for the fabrication of the filters.

REFERENCES

[1] R. E. Collin, *Foundations for Microwave Engineering*. New York, NY, USA: IEEE Press, 1992.
[2] R. E. Collin, *Field Theory of Guided Waves*. New York, NY, USA: IEEE Press, 1991.
[3] G. Matthaei, L. Young, and E. M. T. Jones, *Microwave Filters, Impedance-Matching Networks, and Coupling Structures*. New York, NY, USA: McGraw-Hill, chs. 8–11.
[4] A. Wexler, "Solution of waveguide discontinuities by modal analysis," *IEEE Trans. Microw. Theory Techn.*, vol. 15, no. 9, pp. 508–517, Sep. 1967.
[5] Y.-C. Shih, "Design of waveguide E-plane filters with all-metal inserts," *IEEE Trans. Microw. Theory Techn.*, vol. 32, no. 7, pp. 695–704, Jul. 1984.
[6] H. Patzelt and F. Arndt, "Double-plane steps in rectangular waveguides and their application for transformers, irises, and filters," *IEEE Trans. Microw. Theory Techn.*, vol. 30, no. 5, pp. 771–776, May 1982.
[7] Y. Tang, "Development of substrate integrated waveguide filters," M.S. thesis, Univ. Montreal, Ecole Polytech. Montreal, Montreal, QC, Canada, 2006.
[8] N. Marcuvitz, *Waveguide Handbook*. London, U.K.: Peregrinus, 1986, ch. 4.
[9] S. W. Lee, W. R. Jones, and J. J. Campbell, "Convergence of numerical solutions of iris-type discontinuity problems," *IEEE Trans. Microw. Theory Techn.*, vol. 19, no. 6, pp. 528–536, Jun. 1971.
[10] R. Mittra, T. Itoh, and T.-S. Li, "Analytical and numerical studies of the relative convergence phenomenon arising in the solution of an integral equation by the moment method," *IEEE Trans. Microw. Theory Techn.*, vol. 20, no. 2, pp. 96–104, Feb. 1972.
[11] Y. C. Shih and K. G. Gray, "Convergence of numerical solutions of step-type waveguide discontinuity problems by modal analysis," in *IEEE/MTT-S Int. Microw. Symp. Dig.*, May/Jun. 1983, pp. 233–235.
[12] L. Young, "The quarter-wave transformer prototype circuit," *IRE Trans. Microw. Theory Techn.*, vol. 8, no. 5, pp. 483–489, Sep. 1960.
[13] L. Young, "Stepped-impedance transformers and filter prototypes," *IRE Trans. Microw. Theory Techn.*, vol. 10, no. 5, pp. 339–359, Sep. 1962.
[14] L. Young, "Direct-coupled cavity filters for wide and narrow bandwidths," *IEEE Trans. Microw. Theory Techn.*, vol. 11, no. 3, pp. 162–178, May 1963.
[15] R. Levy, "Tables of element values for the distributed low-pass prototype filter," *IEEE Trans. Microw. Theory Techn.*, vol. 13, no. 5, pp. 514–536, Sep. 1965.
[16] J. D. Rhodes, "Design formulas for stepped impedance distributed and digital wave maximally flat and Chebyshev low-pass prototype filters," *IEEE Trans. Circuits Syst.*, vol. 22, no. 11, pp. 866–874, Nov. 1975.
[17] R. Levy, "Theory of direct-coupled-cavity filters," *IEEE Trans. Microw. Theory Techn.*, vol. 15, no. 6, pp. 340–348, Jun. 1967.
[18] X.-P. Chen and K. Wu, "Recent achievements on substrate integrated waveguide (SIW) filtering structures," in *Proc. Eur. Microw. Conf. Workshop Adv. Topics Design Realization Microw. Filters*, Rome, Italy, Sep./Oct. 2009, pp. 1–42.
[19] X.-P. Chen and K. Wu, "Concept of substrate-integrated circuits applied to filter design and reachable performances," in *Proc. Eur. Microw. Conf. Workshop Recent Adv. Substrate Integr. Waveguide Filters, Simulations Technol. Perform.*, Paris, France, Sep. 2010, pp. 1–30.
[20] X.-P. Chen and K. Wu, "Systematic overview of substrate integrated waveguide (SIW) filters: Design and performance tradeoffs," in *Proc. Asia-Pacific Microw. Conf. Workshop Recent Progr. Filters Couplers*, Yokohama, Japan, Dec. 2010, pp. 1–24.
[21] D. Deslandes and K. Wu, "Single-substrate integration technique of planar circuits and waveguide filters," *IEEE Trans. Microw. Theory Techn.*, vol. 51, no. 2, pp. 593–596, Feb. 2003.
[22] S. B. Cohn, "Design considerations for high-power microwave filters," *IRE Trans. Microw. Theory Techn.*, vol. 7, no. 1, pp. 149–153, Jan. 1959.
[23] X.-P. Chen and K. Wu, "Substrate integrated waveguide filters: Practical aspects and design considerations," *IEEE Microw. Mag.*, vol. 15, no. 7, pp. 75–83, Nov./Dec. 2014.
[24] Y. J. Cheng, K. Wu, and W. Hong, "Power handling capability of substrate integrated waveguide interconnects and related transmission line systems," *IEEE Trans. Adv. Packag.*, vol. 31, no. 4, pp. 900–909, Nov. 2008.

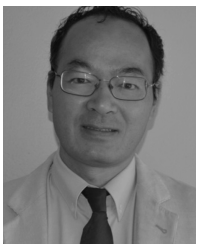

YU (FREEMAN) TANG received the bachelor's and master's degrees in electrical engineering from the University of Electronic Science and Technology of China, in 1985 and 1988, respectively, and the Ph.D. degree in plasma physics for nuclear fusion with a specialization in microwave-plasma interaction physics from the Southwestern Institute of Physics (SWIP), Chengdu, China, in 1995. He was an Associate Research Professor with SWIP from 1995 to 1998. He was a Process Engineer with IBM, Shenzhen (before immigrating to Canada in 1999), an RF Test Engineer and a Microwave Application Engineer with Focus Microwaves, Montreal, QC, and a Researcher with the Poly Gram Research Centre of Montreal in 2002. He was a Filter R&D Engineer with RF Products Inc., NJ (2007 to 2009), specializing in VHF and UHF tunable filters, and a Senior Hardware Developer with Ericsson, Ottawa (2010 to 2013), and Unique Broadband Systems, Toronto (2014). He is currently helping a company in Michigan to push wireless charging products into market. His experience and interests include high power RF filters/duplexer, passive components, switched mode RF amplifier, Doherty amplifier, and subsystem design and development.

KE WU (M'87–SM'92–F'01) received the B.Sc. (Hons.) degree in radio engineering from Southeast University, China, in 1982, the D.E.A. (Hons.) degree in optics, optoelectronics, and microwave engineering from the Institut National Polytechnique de Grenoble, in 1984, and the Ph.D. (Hons.) degree in optics, optoelectronics, and microwave engineering from the University of Grenoble, France, in 1987. He was the Founding Director of the Center for Radiofrequency Electronics Research of Quebec (Regroupement Stratégique of FRQNT). He has been the Director of the Poly-Grames Research Center. He has also held guest, visiting, and honorary professorship with many universities around the world. He is currently a Professor of Electrical Engineering, and the Tier-I Canada Research Chair in RF and Millimeter-Wave Engineering with the University of Montreal, École Polytechnique de Montréal, Canada. He is also interested in the modeling and design of microwave and terahertz photonic circuits and systems. He has authored or co-authored over 1000 referred papers, and a number of books/book chapters and holds 30 patents. His current research interests involve substrate integrated circuits, antenna arrays, advanced CAD and modeling techniques, wireless power transmission and harvesting, and development of low-cost RF and millimeter-wave transceivers and sensors for wireless systems and biomedical applications.

Dr. Wu is a member of the Electromagnetics Academy, the Sigma Xi Honorary Society, and the International Union of Radio Science. He is a fellow of the Canadian Academy of Engineering and the Royal Society of Canada (The Canadian Academy of the Sciences and Humanities). He was a recipient of many awards and prizes, including the first IEEE MTT-S Outstanding Young Engineer Award, the 2004 Fessenden Medal of the IEEE Canada, the 2009 Thomas W. Eadie Medal of the Royal Society of Canada, the 2013 Queen Elizabeth II Diamond Jubilee Medal, the 2013 FCCP Education Foundation Award of Merit, the 2014 IEEE MTT-S Microwave Application Award, the 2014 Marie-Victorin Prize (Prix du Quebec, the highest distinction of Québec in the natural sciences and engineering), and the 2015 Prix d'Excellence en Recherche et Innovation of Polytechnique Montréal. He has held key positions in and has served on various panels and international committees, including the Chair of the technical program committees, international steering committees, and international conferences/symposia. In particular, he was the General Chair of the 2012 IEEE MTT-S International Microwave Symposium. He has served on the editorial/review boards of many technical journals, transactions, proceedings, and letters, and scientific encyclopedia, as Editor and Guest Editor. He is the Chair of the joint IEEE chapters of MTTS/APS/LEOS in Montreal. He was elected as an IEEE MTT-S AdCom Member from 2006 to 2015, and served as the Chair of the IEEE MTT-S Transnational Committee and member of the Geographic Activities Committee and Technical Coordinating Committee, among many other AdCom functions. He is the 2015 IEEE MTT-S President-Elect and will become the 2016 IEEE MTT-S President. He is the inaugural three-year representative of North America as a member of the European Microwave Association General Assembly. He was an IEEE MTT-S Distinguished Microwave Lecturer from 2009 to 2011.

NAZIH KHADDAJ MALLAT (M'07–SM'12) received the B.E. degree in electrical and computer engineering from Lebanese University, in 2000, the master's degree from the Ecole Nationale Supérieure des Télécommunications de Bretagne, France, in 2002, and the Ph.D. degree in telecommunication from the Institut National de la Recherche Scientifique, University of Quebec, Canada, in 2010. After his Ph.D. and till 2012, he was a Post-Doctoral Fellow with the École Polytechnique de Montreal. In 2013, he joined the College of Engineering and Information Technology, Al Ain University of Science and Technology, United Arab Emirates, as an Assistant Professor. He was the Head of the Networks and Communication Engineering and Computer Engineering Department in 2013, and the Deputy Dean of the College of Engineering and Information Technology in 2014. He has effectively taught many courses and their relevant practical elements in laboratories with multiple Montreal universities (ETS, TELUQ, and the École Polytechnique de Montreal). He has authored or co-authored over 20 publications, mostly focused on multiport applications, and millimeter-wave circuits and systems. His main research interests are passive microwave/millimeter-wave circuit design, and telecommunication systems. He is a member of the Ordre des Ingénieurs du Québec. His research results have been presented in international conferences and submitted for journal publication. The Fonds Québécois de la Recherche sur la Nature et les Technologies, a granting agency of the Quebec Government, has awarded him two prestigious scholarships for his Ph.D. studies (2008) and post-doctoral research (2010–2011) thanks to his highest level of achievement. Since 2006, he has been extremely involved with the IEEE Montreal Section. He was the Vice Chair of the IEEE Montreal Section from 2007 to 2008, the Membership Development Chair from 2009 to 2010, and the Section Chair from 2011 to 2012. He served on the steering committee of many IEEE international conferences, such as EPC2007, SMC2007, EPEC2009, CNSR2010, MWP2010, FBW2011, CCECE2012, and IMS2012. He became a member of the IEEE Canadian Foundation in 2012. He is the Founder of the IEEE AAU Student Branch and the IEEE UAE MTT-S Chapter. He is currently the IEEE UAE Technical Activities Coordinator and IEEE Region 8 Chapter Coordination Subcommittee Chair.